CIRP Annals - Manufacturing Technology 60 (2011) 157–160

Contents lists available at ScienceDirect

CIRP Annals - Manufacturing Technology

journal homepage: http://ees.elsevier.com/cirp/default.asp

Hollow needle tissue insertion force model

Jason Z. Moore [a,*], Kostyantyn Malukhin [b], Albert J. Shih [a], Kornel F. Ehmann [b]

[a] Department of Mechanical Engineering, University of Michigan, Ann Arbor, MI 48105, USA
[b] Department of Mechanical Engineering, Northwestern University, Evanston, IL, USA

Sponsored by Stephen Malkin (1), Department of Mechanical and Industrial Engineering, University of Massachusetts, Amherst, MA, USA.

ARTICLE INFO

Keywords:
Force
Cutting edge
Tissue cutting

ABSTRACT

In this study, a mechanistic approach using elementary cutting tool (ECT) edges of varying inclination and normal rake angles is demonstrated to be capable to predict hollow needle insertion force. A needle force model is developed and validated for the specific case of 11 gauge two-plane symmetric needles. Blades of varying inclination and rake angles are inserted into bovine liver to determine the specific force of initial tissue cutting for the given edge geometry; this information is applied to the ECT force model which is validated against experimental force results of hollow needles inserted into bovine liver.

1. Introduction

Hollow needles are among the most widely used medical devices. They are utilized in a wide variety of procedures including biopsy, regional anesthesia, blood sampling, and drug delivery [1]. All of these procedures rely on the ability of the needle to effectively apply force to cut tissue. The geometry of a hollow needle tip determines the distribution of cutting forces. A better understanding of the cutting forces that act on the needle can lead to more effective hollow needle designs and operating procedures and, consequently, improved tissue cutting.

The cutting of soft tissue by a hollow needle is of particular interest in biopsy-based diagnostic procedures in which a tissue sample is removed and examined by a pathologist for abnormalities. End-cut biopsy, shown in Fig. 1(a), uses a hollow needle and a stylet both of which initially jointly advance to the site of the biopsy. The hollow needle then advances further to cut a tissue sample as depicted in Fig. 1(b), while the stylet remains fixed in place. The cutting efficiency in end-cut needle biopsy is characterized by the length of the biopsy samples taken, sample fragmentation, and consistency of the sample lengths [2,3]. Studies have shown that longer and less fragmented biopsy samples allow for more accurate diagnosis [3]. Current end-cut biopsy needles are inconsistent in their performance, sometimes requiring multiple needle insertions to acquire an adequate amount of tissue in particular in prostate cancer biopsy [2]. In addition to the end-cut biopsy example, there are many cases where a better understanding of the forces acting on the needle's cutting edges could potentially improve the efficiency and consistency of biopsy procedures.

Much work has been performed on the study of solid needle insertion. Podder et al. [4] have measured solid needle insertion into tissue. Force and deflection as a function of solid needle geometry has been reported by O'Leary et al. [5]. Furthermore, force and deflection models of solid needle insertion have been developed in a number of studies [1]. These studies, however, cannot be directly applied to hollow needle cutting because the contact length between the hollow needle's edge and tissue is significantly smaller. A survey of the literature shows that results are lacking on understanding the variation of tissue cutting forces along the cutting edges of hollow needles. Yet, it is unquestionable that the knowledge of the tissue cutting forces would offer an indispensible tool in the design of more effective hollow needle tip geometries.

Mechanistic approaches for the prediction of cutting forces have been well established in machining [6]. One of the methods used to develop cutting force models relies on the concept of elementary cutting tool (ECT) edges [7]. In this method, the force that acts on an ECT is determined. The total force that acts on the tool, in turn, is the sum of all ECT forces. The necessary requirements for implementing this approach are the availability of exact tool geometry models and experimentally determined specific cutting force values. To apply the mechanistic approach to needle tissue cutting, analytic expressions for the inclination angle (λ), normal rake angle (α), and contact length for a wide variety of needle tip geometries have been developed by Moore et al. [8–10]. Using these developments as a basis, the goal of this paper is to show that the mechanistic approach based on the ECT concept can be applied to study cutting forces during needle insertion into tissue. To this end, a general needle force model is proposed and then validated for the specific case of 11 gauge two-plane needles. Force insertion experiments with 16 blades of varying geometry into bovine liver are used to establish the relationship between the specific cutting force and the cutting edge angles λ and α.

In Section 2 a synopsis of needle tip geometry modeling is given. Section 3 presents the proposed mechanistic insertion force model. Section 4 explains the experimental setup followed by model validation results in Section 5.

* Corresponding author.

0007-8506/$ – see front matter © 2011 CIRP.
doi:10.1016/j.cirp.2011.03.101

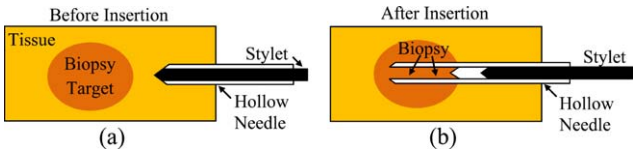

Fig. 1. End-cut biopsy needle.

2. Hollow needle cutting edge rake and inclination angles

Given the mechanics of cutting during needle penetration it is evident that the cutting geometry reflects the general oblique configuration which is uniquely characterized by λ and α. Moore et al. [8,9] have developed analytical expressions for α and λ for a variety of needle configurations including the two-plane symmetric needle illustrated in Fig. 2(a). Fig. 2(b) shows a two-plane symmetric needle whose z-axis coincides with the needle's axis, an x-axis that passes through the lowest point on the needle tip, and γ designating the radial angle of point, A, measured from the x-axis. At point A for a two-plane symmetric needle of bevel angle, ξ, λ, and α can be expressed as [8]:

$$\lambda = \sin^{-1}\frac{|\cot\xi \sin\gamma|}{\sqrt{1+\cot^2\xi\ \sin^2\gamma}} \tag{1}$$

$$\alpha = \cos^{-1}\sqrt{\cos^2\gamma\ \sin^2\xi + \sin^2\gamma} \tag{2}$$

3. Mechanistic approach for cutting force prediction

In the context of this paper the focus will be the determination of the initial cutting force (F_N) upon needle insertion into the tissue. This is the force that is required to initially fracture the tissue bonds and begin penetration. F_N, considering the geometric entities of the needle (Fig. 3(a)), can be considered as the sum of two components: the cutting edge force (F_C) along the needle's inside cutting edge and the force (F_L) acting at its leading edges, i.e.:

$$F_N = F_C + F_L \tag{3}$$

Heverly et al. [11] have experimentally observed that there exists two distinct phases in the evolution of the tissue cutting force. In the first phase (Phase 1) the tissue deflects in the region where the cutting edge pushes on the tissue. This force increases as the tissue deflects; however, no tissue cutting occurs. The second phase (Phase 2), during which the tissue is cut, is characterized by a sudden decrease or leveling-off of the force. These two phases may repeat multiple times. The first transition between the two phases marks the force F_N. A typical insertion force profile depicting the phases is shown in Fig. 3(b).

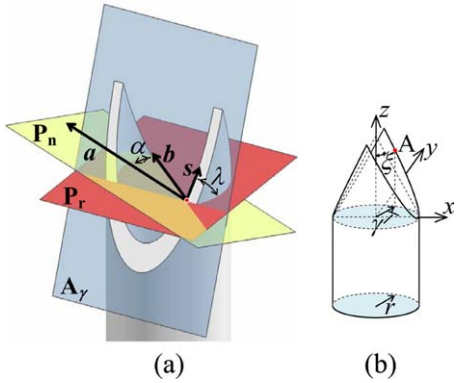

Fig. 2. Two-plane symmetric needle: (a) inclination and normal rake angles on needle tip's cutting edge and (b) line drawing of the needle's cutting edge.

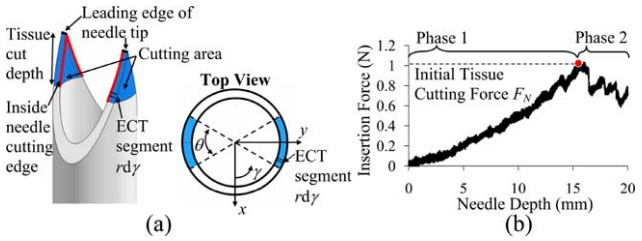

Fig. 3. (a) Leading and cutting needle edges and (b) two phases in needle force insertion into tissue.

In the following sub-sections, based on the ECT concept, analytical expressions for the two constituent tissue cutting force components will be developed.

3.1. ECT force model formulation

Cutting edge force – F_C: To determine F_C based on the ECT concept, the needle's cutting edge is divided into a continuous series of infinitesimal segments having a cutting width equal to $r\,\mathrm{d}\gamma$, as shown in Fig. 3(a). Each $\mathrm{d}\gamma$ section of the needle contributes an infinitesimal force per cut width (specific force) that is a function of the particular segment's λ and α. In accordance with the ECT method, the specific force, $f(\lambda,\alpha)$, needs to be experimentally determined. In the current work this will be accomplished through the use of planar blades with varying λ and α. The resultant inside cutting edge force at the moment of initial tissue cutting is then calculated by integration as

$$F_C = S\int_b^a f(\lambda,\alpha) r\,\mathrm{d}\gamma \tag{4}$$

where a and b denote the range or series of ranges of γ where the needle is in contact with the tissue upon initial tissue facture, r is the radius of the cutting edge, and S is a scaling factor, to be discussed in detail in Section 3.2.

The value of the integration limits in Eq. (4) depends on the region of contact between the needle tip and tissue. If the needle tip is very sharp and long the tissue may cut before complete needle insertion takes place, making a and b not simply 0 to 2π radians, but instead, as illustrated by the two-plane symmetric needle in Fig. 3(a), equal to $a = (\pi + \theta)/2$ and $b = (\pi - \theta)/2$ on one half of the needle, where θ denotes the range of contact between the needle and tissue. Due to symmetry the second half of the needle will contribute the same amount of force.

Leading edge force – F_L: The leading edge force of the needle tip (F_L) must also be considered when calculating the total force on the needle as shown in Fig. 3(a). The λ and α of the leading edge are, λ_{Li} and α_{Li}, respectively, where i denotes the leading edge being examined, when a constant leading edge geometry is assumed which is true of almost all needles. For example, the leading edge of a two-plane symmetric needle has the following geometry: $\lambda_L = 0^\circ$ and $\alpha_L = (\pi/2) - \xi$ for both of the two leading edges, $i = 1$ and $i = 2$. The leading edge force is calculated as

$$F_L = t\sum_{i=1}^{n} f(\lambda_{Li},\alpha_{Li}) \tag{5}$$

where t is the thickness of the needle and $n(>0)$ is the total number of leading edges. For a variable leading edge geometry integration should be applied across the varying geometry of the needle thickness. If there are no specific leading edges, such as in the case of a one-plane needle, then $n = 0$ and therefore $F_L = 0$.

Initial cutting force – F_N: By combining the force components given by Eqs. (3)–(5) a complete model for the determination of the initial cutting force (F_N) for any hollow biopsy needle is given by Eq. (6) and by Eq. (7) for the specific case of a two-plane symmetric

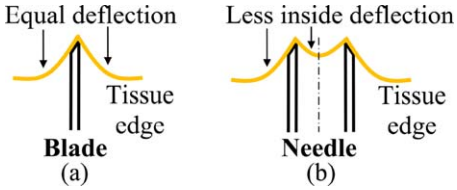

Fig. 4. Higher tissue deviation on (a) blade than on (b) needle.

needle, i.e.

$$F_N = S\int_b^a f(\lambda,\alpha) r\, d\gamma + t\sum_{i=1}^{n} f(\lambda_{Li},\alpha_{Li}) \quad (6)$$

$$F_N = S\int_{(\pi-\theta)/2}^{(\pi+\theta)/2} 2\, f(\lambda,\alpha) r\, d\gamma + 2\, t\, f(0,\frac{\pi}{2}-\xi) \quad (7)$$

F_N neglects the friction force between the tissue and the needle face. This value is not considered because it is small due to the small surface area of the needle's tip cutting face.

3.2. The scaling factor S

The models given by Eqs. (6) and (7) include a scaling factor, S, to take into account, the differences that arise when applying the flat blade model of $f(\lambda,\alpha)$ to predict needle force. It is observed that the blade creates less tissue deflection, Fig. 4(a), than a needle, Fig. 4(b), and thereby utilizes less energy and more efficiently applies force to the tissue than a needle due to its non-curved geometry. The S factor would vary depending on needle diameter, needle thickness, and the level of vacuum applied inside the needle. In our study the S factor is found using a least squares fit to experimental data in Eq. (7).

4. Experimental setup and procedure

The experimental setup, Fig. 5, uses a Siskiyou Instrument's 200cri linear stage, a Kistler 9256A1 piezoelectric force dynamometer, and a tissue holder that, via a pneumatic cylinder, applies a constant pressure of 15.5 kPa on the tissue block to ensure consistent tissue conditions. The blades and needles tested had an identical thickness (t) of 0.25 mm and were made of 316 stainless steel. The blade contact width was experimentally measured to determine specific force.

Two sets of experiments were performed to validate the proposed force model defined by Eq. (7). Both experiments use force data to determine the point of initial tissue cutting, F_N.

Experiment 1: As shown in Fig. 6, 16 flat blades were manufactured with rake and inclination angles that cover a broad range of two-plane symmetric needle geometries, i.e.,

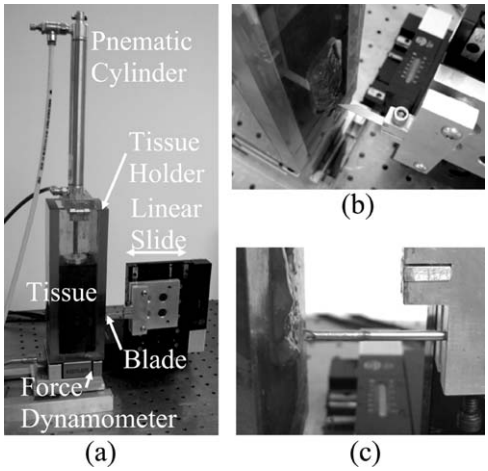

Fig. 5. (a) Overview of the experimental setup, (b) blade cutting of bovine liver, and (c) needle insertion into bovine needle.

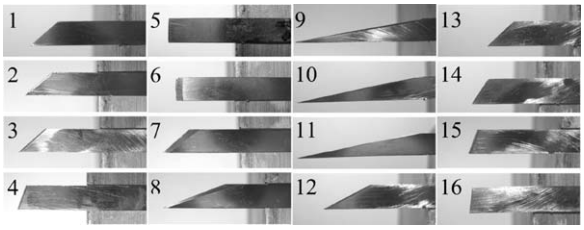

Fig. 6. The 16 blades of varying rake and inclination angles.

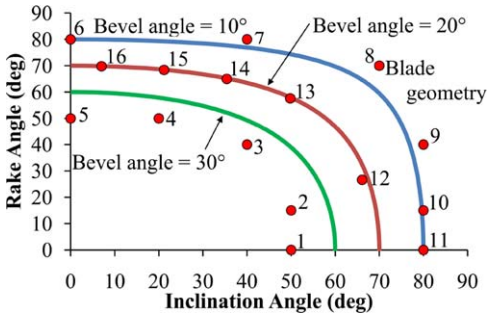

Fig. 7. Inclination and rake angle of 16 experimental blades.

$10^\circ \le \xi \le 30^\circ$ as depicted in Fig. 7. These blades were inserted 10 times each into bovine liver and the cutting behavior was experimentally evaluated. These experiments allowed for the determination of the specific force model $f(\lambda,\alpha)$.

Experiment 2: Five 11 gauge two-plane symmetric needles with bevel angles of 10°, 15°, 20°, 25°, and 30° were each inserted into bovine liver tissue ten times, for a total of 50 trials. The depth of the needle at the point of initial tissue fracture was recorded to determine the relationship between θ and ξ along with the initial cutting force to validate the force model, Eq. (7).

5. Results and discussion

Based on the two sets of experiments $f(\lambda,\alpha)$, $\theta(\xi)$, and S were determined and used to validate the force model.

5.1. Determination of the specific force – f(λ,α)

The dots in Fig. 8 show the average specific force calculated from the blade results in Experiment 1 for given inclination and rake angles. The surface shown in Fig. 8 depicts $f(\lambda,\alpha)$ [N/mm] that corresponds to a 3rd order multivariable (λ and α) best fit polynomial of the data, see Eq. (8). The coefficients were estimated using Matlab for given values of α and λ in radians. The model fits well with an R^2 value of 0.97. The estimated $f(\lambda,\alpha)$ function is valid for needles with bevel angles between $\xi = 10^\circ$ and $\xi = 30^\circ$ because the blades tested were within this range.

$$f(\lambda,\alpha) = -0.042 + 0.296\lambda + 0.298\alpha - 0.255\lambda^2 - 0.408\lambda\alpha - 0.011\alpha^2 + 0.083\lambda^3 + 0.118\lambda^2\alpha + 0.080\lambda\alpha^2 - 0.059\alpha^3 \quad (8)$$

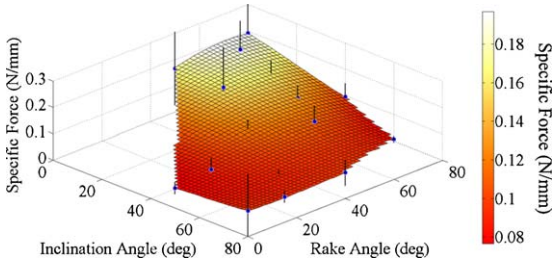

Fig. 8. Mechanistic model from blade results, $f(\lambda,\alpha)$.

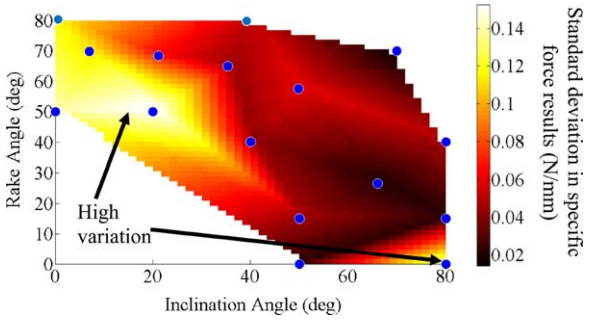

Fig. 9. Standard deviation in blade results.

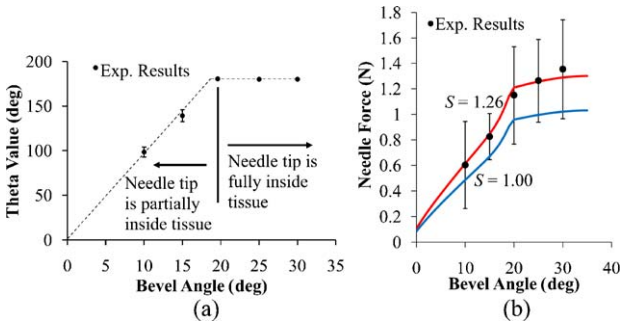

Fig. 10. (a) θ value measured and least squares fit model and (b) force model compared to needle force experimental results.

Fig. 9 shows the standard deviation for the specific force results compared to λ and α with the space between the data points linearly interpolated. It is evident that there is a high variability for low λ and for a combination of low α and high λ. Geometries that cause high variability should be avoided to maximize performance consistency.

5.2. Determination of $\theta(\xi)$

In Experiment 2, θ was found for each of the five needles as shown in Fig. 10(a). A least squares linear curve fit relationship between θ and ξ was found to be:

$$\begin{aligned} \theta &= 9.2\xi \quad \xi < 19.6^\circ \\ \theta &= 180^\circ \quad \xi > 19.6^\circ \end{aligned} \tag{9}$$

5.3. Comparative assessment of predicted and experimental results

The experimentally measured average initial tissue cutting forces for the five needles are given in Fig. 10(b) along with the forces predicted by the needle force model (Eq. (7)) for $S = 1.00$ and 1.26 by utilizing the values that were derived for θ and $f(\lambda,\alpha)$. $S = 1.26$ was found using a least squares fit and is valid for 11 gauge thin walled needles with no vacuum applied. The model has an $R^2 = 0.979$; thereby confirming the validity of the force model for an 11 gauge needle.

To use the general force model expressed by Eq. (6), both S and θ must be experimentally determined. The specific force model, $f(\lambda,\alpha)$ is valid if the needle geometry remains within the range of the λ and α of the tested ECT edges, shown in Fig. 7.

6. Conclusions

A mechanistic approach, using the ECT concept, was used to develop a force model based on λ and α. The approach has demonstrated to accurately predict needle insertion forces. The force model was validated based on experimental force results obtained from five 11 gauge two-plane symmetric biopsy needles thereby proving the concept of using ECTs to develop a needle tip force model. The force model provides insights into the distribution of the tissue cutting forces during needle insertion and can be used to improve needle tip designs for more efficient cutting of tissue and better biopsy outcomes.

The force model developed is shown to have an R^2 value of 0.979 when compared to the actual needle data. It was also found that cutting edges with higher λ cut tissue with lower cutting forces. Cutting edges with low λ (less than 30°) or a combination of high λ (greater than 70°) and low α (less than 10°) are demonstrated to produce a greater variation in cutting forces.

References

[1] Abolhassani N, Patel R, Moallem M (2007) Needle Insertion into Soft Tissue: A Survey. *Medical Engineering and Physics* 29(4):413–431.
[2] Fink K, Hutarew G, Pytel A, Schmeller N (2005) Prostate Biopsy Outcome Using 29 mm Cutting Length. *Urologia Internationalis* 75:209–212.
[3] Ubhayakar G, Li W, Corbishley C, Patel U (2002) Improving Glandular Coverage During Prostate Biopsy Using a Long-Core Needle: Technical Performance of an End-Cutting Needle. *BJU International* 89(1):40–43.
[4] Podder TK, Clark DP, Sherman J, Fuller D, Messing E, Rubens D, Strang J, Brasacchio R, Liao L, Ng WS, Yu Y (2006) In Vivo Motion and Force Measurement of Surgical Needle Intervention During Prostate Brachytherapy. *Medical Physics* 33(8):2915–2922.
[5] O'Leary M, Simone C, Wahio T, Yoshinaka K, Okamura A (2003) Robotic Needle Insertion: Effects of Friction and Needle Geometry. *IEEE International Conference on Robotics and Automation*, 1774–1780.
[6] Ehmann K, Kapoor S, DeVor R, Lazoglu I (1997) Machining Process Modeling: A Review. *Journal of Manufacturing Science and Engineering* 119. 655-663.
[7] Li R, Shih A (2007) Tool Temperature in Titanium Drilling. *Journal of Manufacturing Science and Engineering* 129:740–749.
[8] Moore J, Zhang Q, McGill C, McLaughlin P, Zheng H, Shih A (2010) Modeling of the Plane Needle Cutting Edge Rake and Inclination Angles for Biopsy. *Journal of Manufacturing Science and Engineering* 132. 051005-1-8.
[9] Moore J, Zhang Q, McGill C, Zheng H, McLaughlin P, Shih A. Modeling Cutting Edge Geometry for Plane and Curved Needle Tips, *Proceedings of the Institution of Mechanical Engineers Part B: Journal of Engineering Manufacture*, submitted for publication.
[10] Moore J, Shih A (2010) Tissue Oblique Cutting Flow Angle and Needle Insertion Contact Length. *Transactions of NAMRI/SME* 38:711–718.
[11] Heverly M, Dupont P, Triedman J (2005) Trajectory Optimization for Dynamic Needle Insertion. *International Conference on Robotics and Automation*, 1658–1663.